



# Effects of Nb on microstructure and wear resistance of Fe–Cr–C–B surfacing alloy

Jian Gou<sup>1</sup> · Zheng-jun Liu<sup>1</sup> · Hua Jia<sup>1</sup>

Received: 18 January 2017 / Revised: 18 May 2017 / Accepted: 23 May 2017 / Published online: 9 February 2018  
© China Iron and Steel Research Institute Group 2018

## Abstract

The influence of Nb on the microstructure and wear resistance of the surfacing layer was investigated by using the Fe-based flux-cored wire in the Fe–Cr–C–B system. The microstructure, microhardness and wear resistance properties of the samples were investigated by X-ray diffraction, scanning electron microscopy, microhardness testing and abrasive wear testing, respectively. The results indicate that microstructures of the alloy are composed of martensite, retained austenite,  $M_{23}(C,B)_6$  and NbC. Boride  $M_{23}(C,B)_6$  is distributed along the grain boundaries, while NbC in shape-regular quadrilateral is distributed in martensite. The microhardness is distributed from the substrate to the surfacing layer gradually. NbC significantly improved the wear resistance of surfacing layer.

**Keywords** Flux-cored wire · Surfacing layer · Microhardness · Microstructure · Wear resistance

## 1 Introduction

With the rapid industrial development, wear-resistant materials continue to attract more attention. A variety of wear-resistant materials, such as cast iron, wear-resistant steel and new wear-resistant materials, have been developed [1–3]. Among them, flux-cored wire is one of the most potential new welding materials. The abrasive resistance of flux-cored wire deposits depends on several factors, but mainly on the microstructure, which defines their properties [4]. It is well known that performance of wear-resistant materials is closely associated with the type and distribution of hard phase [5–10]. Some works have been carried out to adjust the composition and diameter of powder-cored wire to meet the engineering requirements. Therefore, seeking a new wear-resistant material is remarkable for industrial production.

Fe–Cr–C alloy is a traditional wear-resistant alloy system, and the  $Cr_7C_3$  hard phase formed in the surfacing layer possesses excellent anti-abrasion performance. In

addition, the Fe–Cr–C system has been used as hardfacing materials because Cr has a high tendency to form hard carbides, and is thus suitable for applications where high wear resistance is required [11–13]. In order to get better performances, a large number of researchers tried to add other alloying elements in Fe–Cr–C system alloy. Boron is an ideal alloying element. According to previous studies [14–16], after added into Fe–B cast alloy, chromium element mainly distributes in the boride. Chromium concentration in boride is approximately 3.82 times as high as that in matrix, which can play a role in strengthening the surfacing layer. In addition, Nb element can be added to generate NbC to achieve high hardness, low density ( $7.79 \text{ g cm}^{-3}$ ), high melting temperature ( $3600 \text{ }^\circ\text{C}$ ) and more negative standard Gibbs free energy of formation [17]. Therefore, NbC is also a good hard phase to improve strength and wear resistance. Boron and niobium seem to be the ideal additive for improving the hardness and wear resistance of iron-based alloys.

Herein, we try to add ferroniobium alloys in the Fe–Cr–C–B system. The objective of this paper is to study the microstructure, microhardness and wear resistance of the surfacing layer.

✉ Zheng-jun Liu  
liuzhengjun1962@163.com

<sup>1</sup> Department of Material Science and Engineering, Shenyang University of Technology, Shenyang 110870, Liaoning, China

**Table 1** Chemical composition of experimental steel strip (wt%)

C	Si	Mn	S	Ni	P	Cr	Cu	Fe
< 0.01	< 0.03	0.35–0.55	≤ 0.03	≤ 0.3	≤ 0.03	< 0.2	< 0.2	Balance

**Table 2** Chemical compositions of Fe–B, Fe–Nb and Fe–Cr (wt%)

Material	B	Nb	Cr	C	Si	P	Mn	S	Fe
Fe–B	19.29	–	–	0.40	0.38	0.048	–	0.014	Balance
Fe–Nb	–	60.56	–	0.01	0.04	0.010	0.01	0.010	Balance
Fe–Cr	–	–	60.9	8.15	1.15	0.028	–	0.030	Balance

**Table 3** Chemical composition of flux core (wt%)

Sample	C	Cr	B	Nb	Fe
No. 1	10.0	25.0	1.5	0.0	Balance
No. 2	10.0	25.0	1.5	3.0	Balance
No. 3	10.0	25.0	1.5	3.6	Balance
No. 4	10.0	25.0	1.5	4.2	Balance

## 2 Experimental

The flux-cored wire consists of powder and steel strip. The material of steel strip is H08A (10.0 mm × 0.3 mm), and its chemical composition is shown in Table 1. A powder mixture of ferroboron, ferroniobium, ferrochromium alloy and crystalline graphite (99.9% purity) was used as surfacing alloy. The chemical compositions of Fe–B, Fe–Nb and Fe–Cr are presented in Table 2. According to a certain proportion, the powder is mixed evenly and dried. The flux-cored wire was made by wire-making machine assembly line. Table 3 shows chemical composition of the flux core.

The filling rate of the welding wire is set to 45%. In order to verify the accuracy of the filling rate, a finished wire weighing was selected (total weight of 152.12 g and internal powder weight of 67.85 g). The results show that the actual filling rate is 44.6%.

Arc surfacing welding on Q235 steel plate was carried out using a submerged arc welding machine. The welding parameters were as follows: arc voltage of 25–30 V, welding current of 180–200 A, traveling speed of 10 mm s<sup>-1</sup> and wire length of 15 mm. The phases were identified by X-ray diffraction (XRD) analysis, and the morphology of the surfacing layer and wear was observed using a scanning electron microscope (SEM). Microhardness analysis was conducted to measure the hardness of the hard phase in the surfacing layer, with load of 0.98 N and loading time of 10 s.

The abrasive wear test was carried out on the MLS-23 wet rubber wheel abrasive wear tester. The sample size was 56 mm × 27 mm × 11.5 mm, and the test was conducted with the rubber wheel diameter of 150 mm and rubber wheel speed of 240 r/min. The test mortar contains 1000 g water and 1500 g abrasive, and the wear time is 3 min.

## 3 Results and discussion

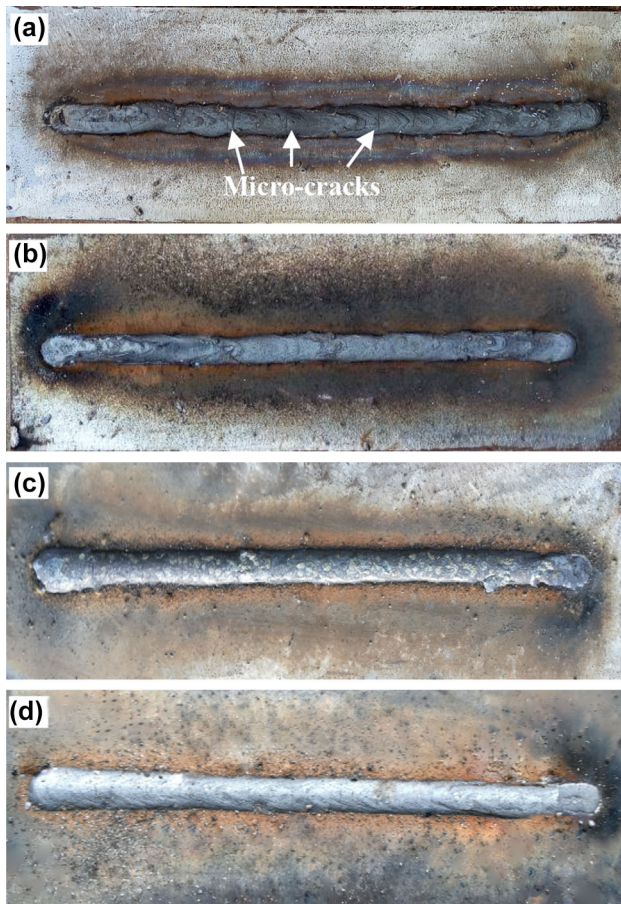
### 3.1 Macro-morphology

Figure 1 shows the macro-morphology of four samples of surfacing layer. It can be seen that the element content affects the weld shape. When there is no Nb addition, the surface of the surfacing layer appears micro-cracks. The cracks on the surface of the surfacing layer are reduced when Nb exists. The Nb content has no obvious difference on the macroscopic topography. On the whole, the surfacing layer of the last three groups showed excellent weld appearance.

Table 4 shows the chemical composition of hardfacing alloy layer. The two layers of the surfacing welding can reduce the dilution effect of the base metal to make the alloy have a better transition. All elements are at a reasonable level. Among them, the existence of boron and carbon in the surfacing layer could influence the structure and affect thermal cracking resistance of surfacing alloy, and the element contents in Table 2 can play a role in strengthening the surfacing layer and thus avoiding the surface cracking.

### 3.2 X-ray spectra and thermodynamic analysis

The microstructure of the surfacing layer, which determines the mechanical properties of the surfacing layer, was studied. Figure 2 shows the XRD spectra of surfacing layer. The phase of sample No. 1 is composed of  $\gamma$ -Fe and M<sub>23</sub>(C,B)<sub>6</sub>. The microstructures of the other three samples



**Fig. 1** Photograph of the surface of surfacing layer. **a** Sample No. 1; **b** sample No. 2; **c** sample No. 3; **d** sample No. 4

**Table 4** Chemical compositions of hardfacing alloy layer (wt%)

Sample	C	Cr	B	Nb	Fe
No. 1	1.48	10.56	0.25	–	Balance
No. 2	1.45	12.49	0.22	0.93	Balance
No. 3	1.29	11.63	0.17	1.15	Balance
No. 4	1.37	12.27	0.24	1.32	Balance

are similar. The results of X-ray analysis show the microstructures of samples No. 2, No. 3 and No. 4 are composed of martensite (M), retained austenite ( $\gamma'$ ),  $M_{23}(C,B)_6$  and NbC, which indicates that  $M_{23}(C,B)_6$  and NbC carbides could be in situ synthesized during self-shield open arc welding process.

During the welding process, the thermodynamics function of the chemical reaction of Nb and C can be described as follows:

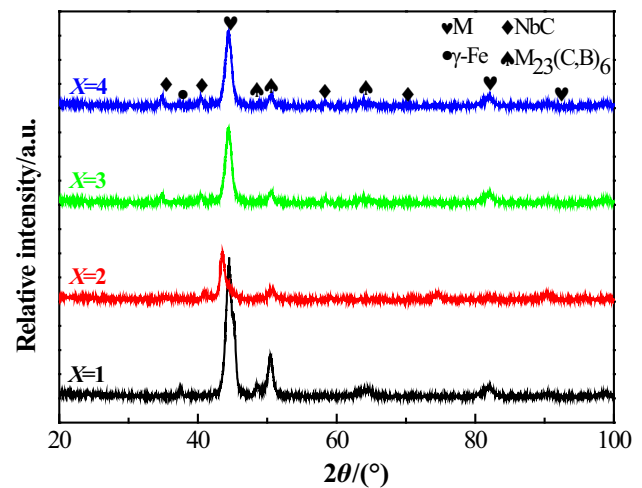
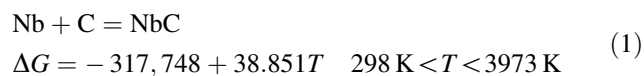


**Fig. 2** XRD spectra of surfacing layer

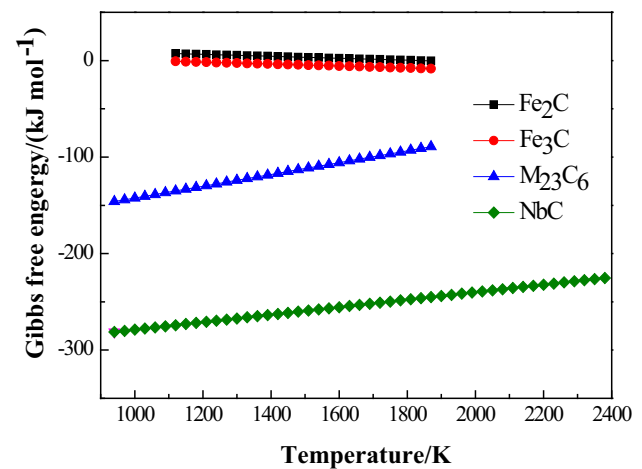
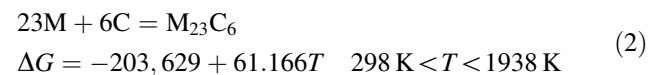


**Fig. 3** Gibbs free energy of reaction

where  $T$  is absolute temperature. The thermodynamic reaction between Fe, Cr and C can be described as follows [18]:



The Gibbs free energy and temperature curves of some kinds of carbides in the surfacing layer are shown in Fig. 3 [19]. As can be seen, the Gibbs free energy of NbC is negative, which indicates that the NbC can be generated spontaneously in the reaction when the element meets the requirement of the compound generation. The very fast heating in the welding process results in a limited number of NbC. The Gibbs free energies of  $Fe_3C$  and  $Fe_2C$  are greater than zero, which shows that there are no stable  $Fe_3C$  and  $Fe_2C$  in the surfacing layer. Figure 3 also shows the feasibility of  $M_{23}C_6$  in situ synthesis. Among them, M stands for Cr and Fe atoms. Due to the low solubility of B in  $\alpha$ -Fe, the B atom is easy to enter the  $M_{23}C_6$

to replace the C atom. It is worth noting that when the Nb element exists, a part of Nb will produce solid solution strengthening into  $M_{23}(C,B)_6$  borides. Therefore,  $M_{23}(C,B)_6$  in the present study is a kind of complex compound. The authors have not been able to find thermodynamic data that support the formation of  $M_{23}(C,B)_6$  under the present conditions, but the microstructure and XRD results also demonstrated the presence of this substance.

In all the products, the Gibbs free energy of NbC is the lowest. As the molten bath cooled, NbC firstly precipitates from liquid phase, and  $M_{23}(C,B)_6$  was generated at the grain boundary with decreasing the temperature. As mentioned above, the residual melt decomposes to fine eutectic carbides and austenite at the eutectic temperature, and then this austenite is retained down to room temperature as a metastable phase. At the final stage of the austenite to martensite transformation, the matrix microstructure is retained as martensite and retained austenite.

### 3.3 Microstructure

Figure 4 shows SEM images for surfacing alloys with different Nb contents. The microstructure of sample No. 1 was composed of white and black phases. Boron solubility is very low in austenite and ferrite, and boron has the characteristics of segregation to grain boundaries. The white and black phases are the boride and substrate, respectively. As shown in Fig. 4b, it contains much regular quadrangular structure and a small quantity of dot and spike structure, and there is network crystal structure near the white bright area in surfacing layer obviously. According to the results of XRD, it can be concluded that white bright phases are NbC and the fine dark gray network phases are  $M_{23}(C,B)_6$ . The dot and spike structure got continuous enrichment of Nb and C elements. The NbC phase continuously grew up, leading to the decrease in the C content in the remaining liquid phase, and boride was discontinuously dispersed along the grain boundary. The

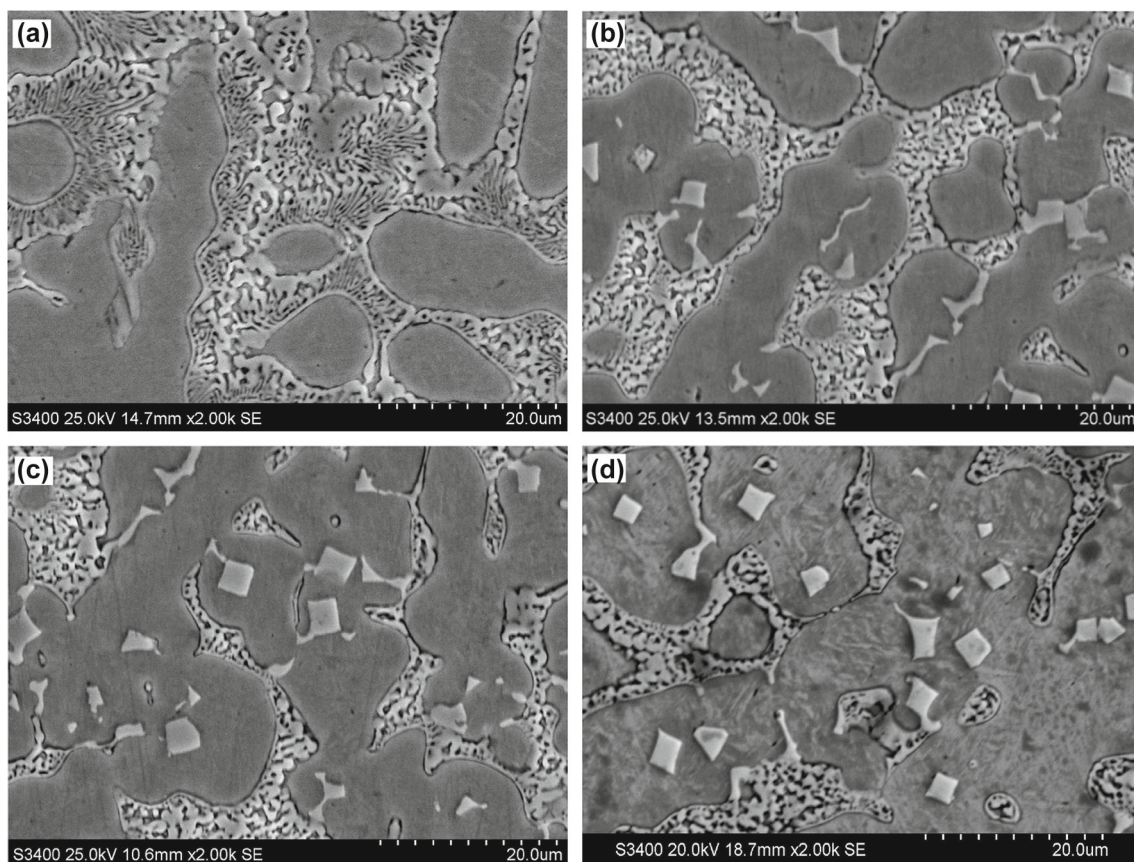


**Fig. 4** SEM images for surfacing alloys with different Nb contents. **a** Sample No. 1; **b** sample No. 2; **c** sample No. 3; **d** sample No. 4

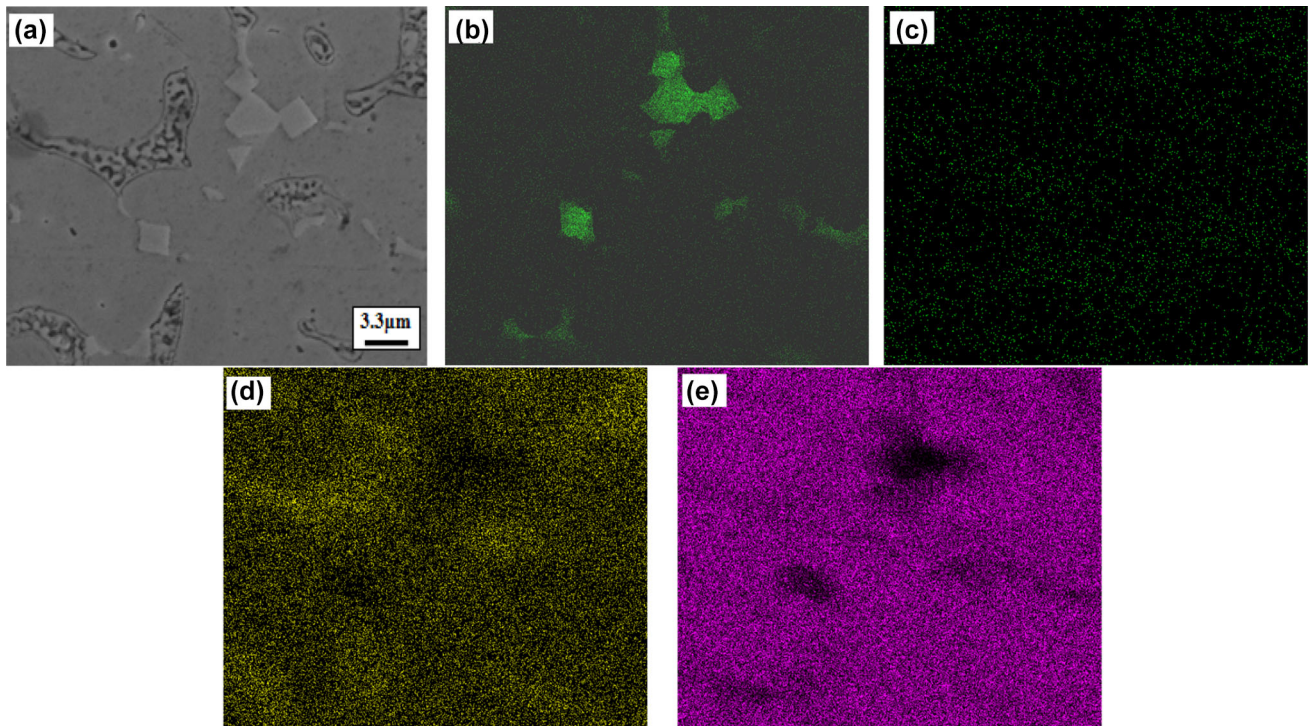


**Fig. 5** Distribution of element in microstructure of surfacing layer. **a** SEM image of carbides; **b** Nb; **c** C; **d** Cr; **e** Fe

reduction in surface energy of the molten pool is the major driving force for small grains to dissolve and large grains to grow.

Figure 5 is the results of energy-dispersive spectroscopy mapping, which shows the distribution of elements in the surfacing layer. It can be seen that the bright and white structure is enriched with Nb and C elements, and combined with the above XRD analysis, it should be the NbC hard phase. It shows that the Cr element is distributed along the grain boundaries; besides, a large amount of C element and a small amount of Fe element are distributed in the grain boundary. As indicated in Fig. 3, the complex carbide  $M_{23}(C,B)_6$  was proved to exist in the grain boundary. Fe element is distributed in gray areas, while the contents of the other three elements in the gray area are very small. Therefore, the gray martensite solid solution with a small amount of Cr element can strengthen the alloy efficiently. Microstructure of the surfacing layer is fine and uniform, leading to excellent strength and toughness and reducing the possibility of crack and micro-spalling in the

wear process. Therefore, the surfacing layer exhibits excellent wear resistance.

Figure 6 shows the morphology of carbide after deep corrosion. After etched in 10% nitric acid alcohol for 12 h, the morphology of the hard phase can be observed. NbC is a three-dimensional structure.  $M_{23}(C,B)_6$  is perpendicular to the surface of the surfacing layer and is embedded in it. The two kinds of hard phases grow independently, which can protect the matrix effectively.

### 3.4 Microhardness

The samples were tested for hardness from the outermost layer to the substrate and measured each point in a step of 0.1 mm perpendicular to the surfacing layer. Figure 7 describes the microhardness profiles of surfacing layers across the interface. The microhardness of surfacing layer of sample No. 1 was about 800 HV. In contrast, the microhardness increases as the Nb content increases up to 4.2%. The two kinds of hard phases  $M_{23}(C,B)_6$  and NbC

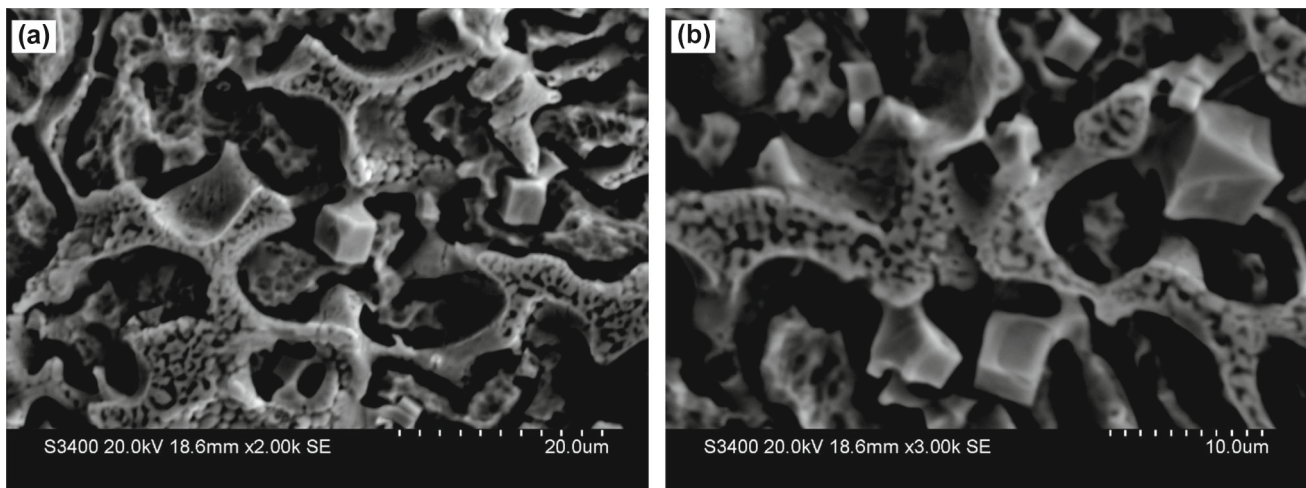


Fig. 6 Low-magnification (a) and high-magnification (b) morphologies of carbide after deep corrosion

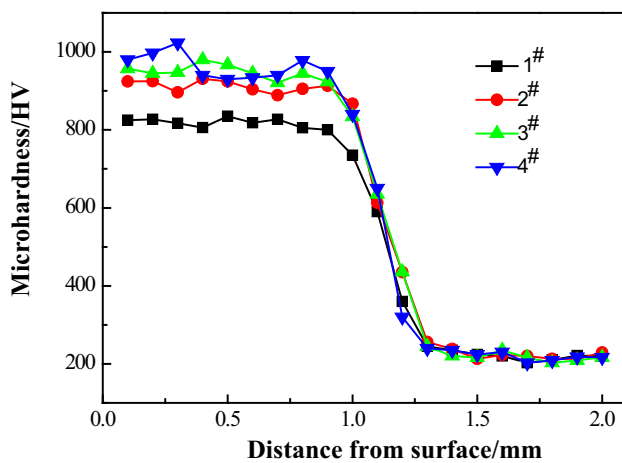


Fig. 7 Microhardness distribution of surfacing layer

can achieve a finer and more uniform microstructure of surfacing layer, especially in the non-equilibrium rapid solidification process; thus, the surfacing layer has high microhardness, which is generally from 930 to 1023 HV. However, near the bottom of the surfacing layer, the hardness of the surfacing layer is gradually reduced to the hardness of the base material due to the dilution effect of the substrate to the surfacing layer. The surfacing layer has high hardness and reasonable gradient distribution, which will ensure the high bonding strength between the surfacing layer and the substrate. During the abrasive wear process, the high-strength surface atom bonding force is big, and the transfer is not easy to happen. Surface-strengthening process can provide a high toughness layer, which significantly improves the ability to resist abrasive wear.

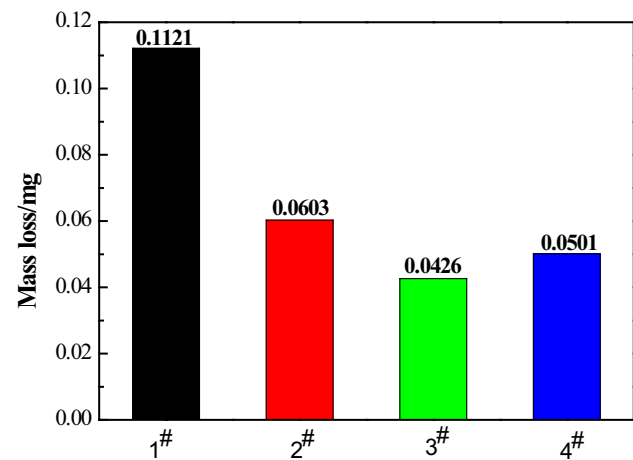
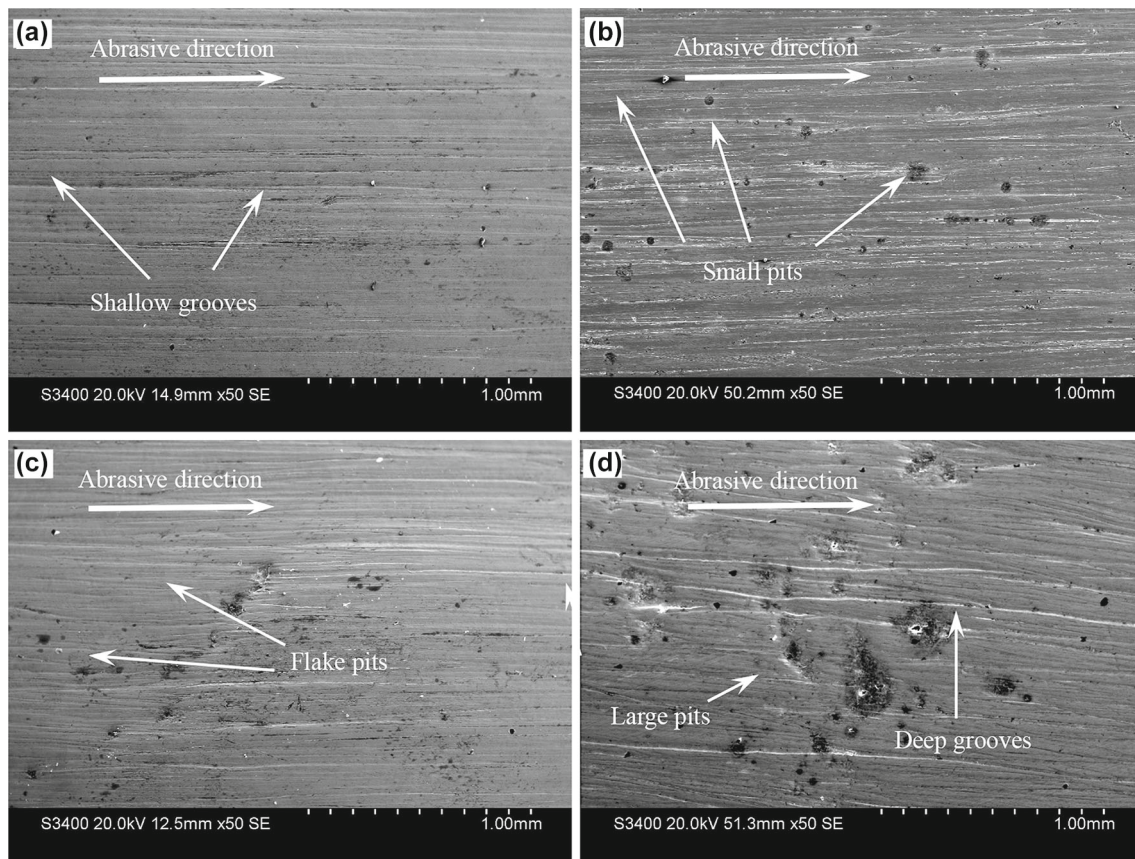


Fig. 8 Mass loss of surfacing layer after abrasion

However, only parts of NbC particles were captured by the solid–liquid interface of martensite and went inside it. Thus, NbC particles were less at the bottom of the molten pool.

### 3.5 Abrasion test

Figure 8 shows the mass loss of every surfacing layer after abrasion. The mass loss of sample No. 1 is 0.1121 g. After the addition of Nb element, the wear quantity was improved significantly. It is worth noting that two kinds of hard phases can be found in the surfacing layer. It is very significant for the improvement in hardness and wear resistance of the surfacing layer. The wear amount decreases first and then increases with the increase in Nb



**Fig. 9** Wear morphology of specimen No. 3 at different time. **a** 3 min; **b** 6 min; **c** 9 min; **d** 12 min

content. This phenomenon is caused by hard phase peeling off along with the secondary cutting, which could increase the resistance.

The wear mechanism was studied by selecting the sample No. 3 with the least mass loss of wear, and the wear morphology was observed every 3 min. Figure 9 shows the wear morphology of specimen No. 3 at different time. When the wear time is 3 min, a number of shallow grooves appeared in the surfacing layer with a slight plastic deformation. As the wear progresses, a small peeling-off pit appears in the surfacing layer. In Fig. 9c, a number of flakes that pit in the surfacing layer can be observed. When the wear time is 12 min, worn surface is composed of deep grooves and pits.

Figure 10 shows the wear principle diagram of surfacing alloy. Figure 10a is a cross-sectional view of sample No. 3, and it can be seen that the structure of the surfacing layer is

composed of matrix, NbC and  $M_{23}(C,B)_6$ , where NbC is a regular rectangle and  $M_{23}(C,B)_6$  is a strip shape. As shown in Fig. 10b, at the beginning of wear, the abrasive wheel is brought into contact with and rubbed on the surface of the surfacing layer, and the first yielded structure is the matrix. As wear progresses, flaking boride precipitates along the grain boundaries and forms a flake pit. Because of the highest microhardness of NbC, the fracture of NbC was formed in the last stage. As shown in Fig. 10d, NbC, matrix and boride fall off together to form a peeling pit. At the same time, shallow grooves transform to deep grooves. A large number of NbC and  $M_{23}(C,B)_6$  staggered and interspersed, building wear-resistant skeleton and leading to the tortuous propagation path, and then resulting in increasing resistance. Thus, the surfacing alloy No. 3 shows excellent wear resistance.

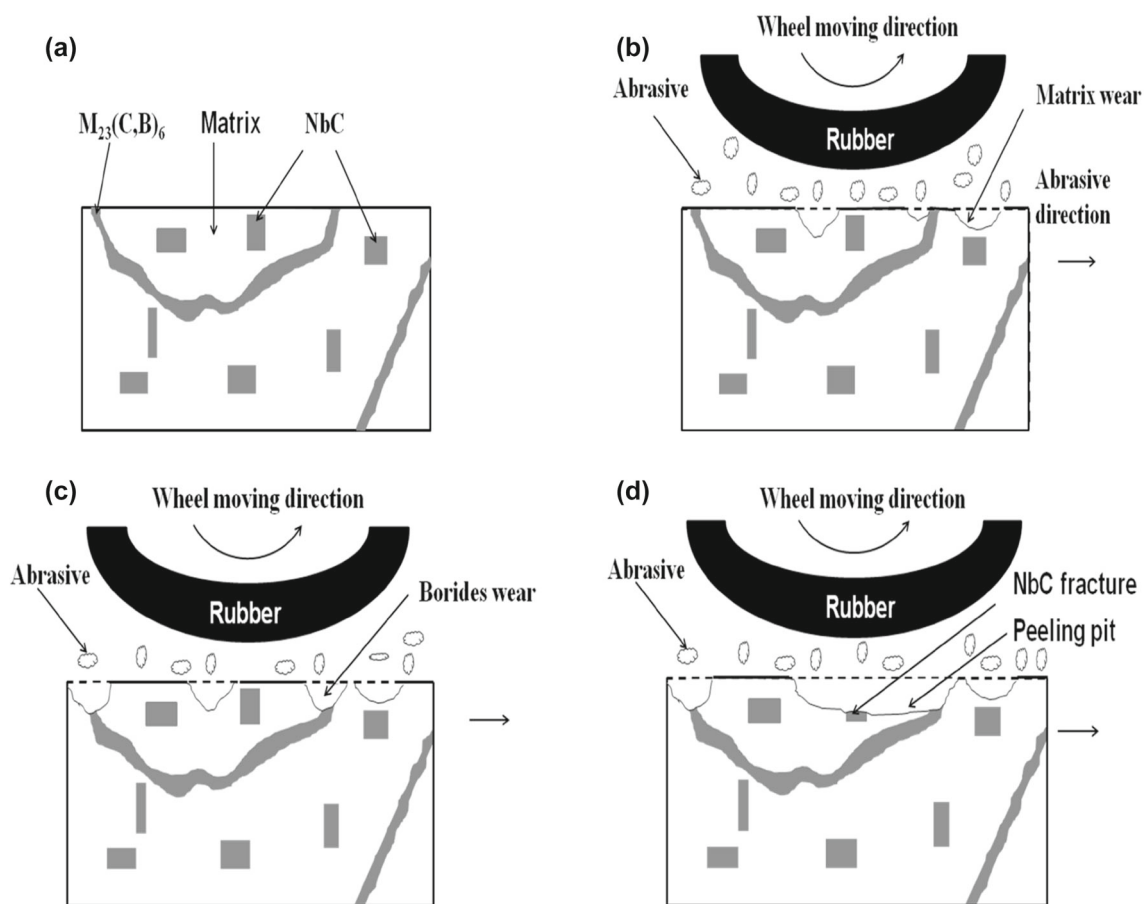


**Fig. 10** Wear principle diagram of Fe–Cr–C–B–Nb surfacing alloy. **a** Section of sample; **b** matrix wear; **c** borides wear; **d** NbC fracture

## 4 Conclusions

1. Proper addition of Nb element can reduce the microcrack of Fe–Cr–C–B alloy. The microstructure of hardfacing alloy is martensite + retained austenite +  $M_{23}(C,B)_6$  + NbC. The feasibility of in situ synthesis of NbC was proved from the thermodynamic point of view.
2. The boride along the grain boundaries is  $M_{23}(C,B)_6$ . Quadrangular structure enriched with Nb and C elements is identified to be NbC. Hardness values varied from 930 to 1023 HV. The surfacing layer has high hardness and reasonable gradient distribution.
3. The in situ synthesis of NbC reduces the amount of wear. The process of wear is followed by three steps, substrate wear, boride wear and NbC fracture.

**Acknowledgements** This work was financially supported by Doctor Foundation Start-up Project of Liaoning Province (No. 20131079).

## References

- [1] X.H. Gao, Z.M. Guo, Q.F. Geng, P.J. Ma, G. Liu, *Sol. Energy Mater. Solar Cells* 157 (2016) 543–549.
- [2] Z.Z. Fu, R. Koc, *Mater. Sci. Eng. A* 676 (2016) 278–288.
- [3] O.P. Modi, D.P. Mondal, B.K. Prasad, M. Singh, H.K. Khaira, *Mater. Sci. Eng. A* 343 (2003) 235–242.
- [4] A. Gualco, H.G. Svoboda, E.S. Surian, *Wear* 360–361 (2016) 14–20.
- [5] H.Y. Liu, Z.B. Song, Q. Lao, S.P. Chen, Q.S. Meng, *J. Alloy. Compd.* 23 (2016) 276–280.
- [6] Q.T. Li, Y.P. Lei, H.G. Fu, Z.W. Wu, J. Lin, *J. Alloy. Compd.* 23 (2016) 124–129.
- [7] S. Yoshioka, L. Boatema, S.V.D. Zwaag, *J. Eur. Ceram. Soc.* 36 (2016) 4155–4162.
- [8] Z.R. Li, D.Y. Li, N.N. Zhang, H. Huang, X. Wang, *J. Alloy. Compd.* 23 (2016) 834–841.
- [9] Y.H. Liu, J. Li, F.Z. Xuan, *Surf. Eng.* 28 (2013) 560–563.
- [10] A. Surzhenkov, M. Antonov, D. Goljandin, P. Kulu, M. Viljus, R. Traksmaa, *Surf. Eng.* 32 (2016) 624–630.
- [11] A. Singh, N.B. Dahotre, *J. Mater. Sci.* 39 (2004) 4553–4560.
- [12] T. Sun, R.B. Song, X. Wang, P. Deng, C.J. Wu, *J. Alloy. Compd.* 22 (2015) 84–90.
- [13] A.P. Modi, *Tribol. Int.* 40 (2007) 490–497.
- [14] Y. Jian, Z. Huang, J. Xing, X. Liu, L. Sun, B. Zheng, *Wear* 362–363 (2016) 68–77.



- [15] J.A. Cabral Miramontes, J.D.O. Barceinas Sánchez, F. Almeraya Calderón, A. Martínez Villafañe, J.G. Chacón Nava, J. Mater. Eng. Perform. 19 (2010) 880–884.
- [16] S.G. Huang, J. Vleugels, H. Mohrbacher, M. Woydt, Metal Powder Rep. 71 (2016) No.5, 349–355.
- [17] J.H. Kim, K.H. Ko, S.D. Noh, G.G. Kim, S.J. Kim, Wear 267 (2008) 1415–1419.
- [18] Y. Yang, J.T. Busby, J. Nucl. Mater. 448 (2014) 282–293.
- [19] L. Zong, Z.J. Liu, Adv. Mater. Res. 189–193 (2011) 518–522.